Composite Structures 345 (2024) 118394

Contents lists available at ScienceDirect

Composite Structures

journal homepage: www.elsevier.com/locate/compstruct

Experimental tensile testing of the lap joint composite laminates supported with the acoustic emission and machine learning techniques

Rayane El Mohtadi [a,*], Jakub Rzeczkowski [b], Izabela Korzec-Strzałka [c], Sylwester Samborski [c], Francesco Aymerich [a], Aleksander Czajka [c]

[a] Department of Mechanical, Chemical and Materials Engineering, University of Cagliari, 09123 Cagliari, Italy
[b] Faculty of Mathematics and Information Technology, Lublin University of Technology, Nadbystrzycka 38d, 20-618 Lublin, Poland
[c] Faculty of Mechanical Engineering, Lublin University of Technology, Nadbystrzycka 38d, 20-618 Lublin, Poland

ARTICLE INFO

Keywords:
Lap joint composite laminates
Tensile testing
Acoustic emission
Machine learning
Fractographic analysis

ABSTRACT

This paper investigates tensile behavior of through thickness reinforced carbon/epoxy lap joint composite laminates, reinforced with steel z-pins and staples, arranged in two rows parallel to the overlapping edges, via experimental testing. Acoustic emission (AE) monitoring is employed during the displacement-controlled tensile tests to monitor damage propagation during loading using the Vallen AMSY-5 measurement system, with two piezoelectric sensors being mounted at the laminate surface. Furthermore, machine learning algorithms are integrated to process AE data, enabling the recognition and prediction of failure mechanisms. Fractographic analyses were performed to observe the nature of damage post-failure. The experimental research was enriched with capturing high-resolution pictures of total crack propagation length growth using a high-resolution photocamera. The performed empirical tests demonstrated that the unstable propagation of a crack along the bonding interface has led to an eventual breakdown of both unreinforced and reinforced joints. An increase in the full displacement and load at failure was clearly detected for both z-pins and staples with a noticeable decrease in crack growth length, while a higher performance was illustrated for staples in comparison to z-pinned and unpinned.

1. Introduction

Carbon fiber-reinforced polymers (CFRPs) have been in the research focus for few decades due to their remarkable strength and stiffness. The excellent mechanical properties of these materials along fiber axis empower designers to meticulously shape their internal structures for specific loading conditions which sets them apart from isotropic materials making them highly implemented in various industry sectors. Because of these unique benefits, composites are widely used to create aircraft and automotive components, which represents a major advancement in cutting-edge technical solutions. The investigation of innovative connecting configurations has gained momentum due to the expanding scale of composite structures. The emphasis is especially on configurations that can survive the diverse range of challenges presented by different loadings, creating a dynamic environment where joining technology developments are critical to the development of strong and durable structures. Adhesive joining is generally the method of choice for attaching thin composite adherends [1,2]. Even though carbon fiber polymer matrix composites have a long history, a recurring problem that restricts their widespread application is the high stress that develops at the joint interface, which leaves them susceptible to through thickness damage like delamination and debonding. This may result in significant reductions in the overall strength and stiffness of the structures, which may cause catastrophic failures without any warning signs [3–5]. To overcome their problems with low delamination resistance and poor impact damage tolerance, several 3D fiber composites have been developed [6,7]. In particular, the performance of 3D fiber composites is greatly improved by the use of through thickness fibers, or z-binders [8,9]. Many strengthening methods have been investigated to improve the structural integrity of bonded or co-cured composite joints in order to produce 3D preforms. Of them, z-pinning has emerged as a z-reinforcement method that works well for uncured prepreg laminates. Inserting thin metal or carbon rods into the through thickness direction is the z-pinning approach [10–16]. A number of studies looked at the performance of lap joints reinforced with a different hybrid method, in which two prepreg adherends are separated before consolidation by a

* Corresponding author.
E-mail address: rayane.elmohtadi@unica.it (R. El Mohtadi).

https://doi.org/10.1016/j.compstruct.2024.118394
Received 29 March 2024; Received in revised form 1 June 2024; Accepted 15 July 2024
Available online 16 July 2024

thin metal sheet with protruding spiky pins [17–22]. The beneficial effect resulted from the traction forces that are transmitted by the through thickness z-reinforcement along the delamination crack. These forces increased resistance to crack propagation by actively opposing crack opening and sliding [12,23]. Z-pinning has demonstrated its ability to improve through thickness mechanical properties of the structures, such as interlaminar fracture resistance, ultimate strength, resistance to delamination, and damage tolerance, while also lowering the susceptibility to structural failure in comparison to alternative methods [10]. According to research by Cartié et al., under modes I and II loadings, the bridging effects made possible by z-pins can increase delamination resistance by as much as 160 % and 100 %, respectively [24]. Zhang and colleagues stated that the increased delamination toughness reduces the damage area induced by impacts in addition to increasing impact resistance. Impact damage areas on z-pinned laminates, for example, are up to 64 % less than on unpinned laminates. Additionally, the authors discovered that the effectiveness of z-pinning is greater in containing the spread of delamination rather than in initiating damage [25]. Mouritz and researchers found that applying z-pinning across the bonding surfaces significantly improved the failure strength and energy absorption of lap, T-shaped, and L-shaped composite joints [26,27]. Among composite adherends, z-pinning has proven to be remarkably effective in increasing the tensile strength of various lap joint designs [10,28,29]. The strength of single-lap carbon/epoxy adherends was examined in relation to metal inserts with three different patterns of steel pins (with pins evenly dispersed over the overlap region, concentrated near the overlap edges [22]. When subjected to a tensile loading with varying z-pin content, Chang and colleagues observed a significant improvement in the ultimate strength and fatigue life of lap joints reinforced with z-pins [26]. Several crack-stopping approaches were under investigation like rivetless nut plates [30], small diameter pins [31]. The initial phase of technology assessment, which showcased the possibilities of stapled joints, was carried out by Löbel et al. [31], when compared to bolted joints, stand-alone staples showed an overall 28 % increase in tensile strength. Comparing patented edge-staple joints to solely bonded joints, there was a 23 % gain in tensile strength. Due to the lack of pullout, the geometric shape of staples offered an efficient method of axial attachment [31]. Through thickness rods or pins across composite adherends can cause distinct mechanisms of damage and deformation under load, which have been experimentally seen and described in [32]. Because the damage accumulation in CFRP composites is usually internal and does not show up any visible signs on the surface of the structure, assessing the damage can be difficult [33]. There is a wide variety of non-destructive testing methods available for composite constructions, including X-ray tomography [34], ultrasonic testing [35], eddy current testing [36], and infrared tomography [37]. As an example, some authors examined the use of X-ray tomography in composite structure damage imaging [38–40]. The goal of the study was to locate fiber breakage, matrix cracking, and delamination in composite materials [41]. One of the most promising of these is the acoustic emission (AE) method, which has been applied in a number of ways as a real-time monitoring tool to follow the behavior of composite structures [33]. High accuracy defect region localization is possible using the AE approach. Numerous studies and publications have been done in the literature regarding the application of the acoustic emission technique to the localization of flaws in composite materials [42]. The acoustic emission (AE) approach shows remarkable sensitivity and reliability when it comes to identifying active cracks [43], especially in the early stages of their initiation [44]. The characteristics of AE transients resulting from different failure modes in CFRP composites, such as matrix cracking, delamination, fiber fracture, and debonding, have been the subject of numerous research studies [45–47]. Using the time of arrival (TOA) method, which is based on examination of the difference in registered arrival time of transient stress wave acquired by succeeding sensors, the AE events created by propagating failure are located. However, the TOA technique's application can result in measurement

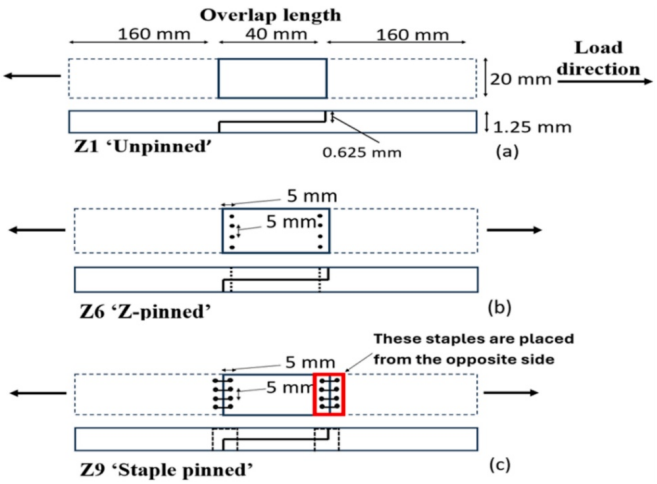

Fig. 1. Geometry and groups of single step joints samples (dimensions not to scale): (a) Unpinned lap joint (Z1), (b) Z-pinned lap joint (Z6), and (c) Staple pinned lap joint (Z9).

inaccuracies because of the dispersive nature of propagating Lamb waves and important material attenuation qualities. Consequently, numerous investigators experimented with different approaches for localizing defects [48,49]. Lately, AE data has been analyzed using several kinds of machine learning methods to categorize the damage modes in composite laminates. Several types of damage occurring in open hole tensile specimens (OHT) were assessed using the k-means clustering approach by Ozaslan et al. [50]. The study conducted by Xu et al. [51] employed the *k*-means++ clustering technique to detect distinct damage patterns in laminate subjected to hygrothermal aging in a single lap joint. Godin et al. [47] clustered the damage modes in GFRP composite laminate under tensile strain using a combination of *k*-means and *k*-nearest neighbor algorithms. In order to anticipate the failure load under stress, Sause et al. [52] suggested an artificial neural network (ANN)-based AE method. The damage modes that are occurring in a buckled CFRP panel were located and classified by McCrory et al. [53]. The damage in quasi-isotropic laminates under indentation was classified by Saeedifar et al. [54] using a wide range of clustering techniques, including fuzzy C-Means, k-means, genetic k-means, Self-Organizing Map (SOM), Gaussian Mixture Model (GMM), and hierarchical model. The CFRP laminate failures under fatigue load were characterized by Bhat et al. [55] using ANN to remove noise resulting from AE signals. Determining the ideal number of clusters to classify the damage is the main challenge with clustering algorithms.

The aim of this paper is to understand how the through thickness pinning reinforcement process influences the initiation and propagation of damage in the material. The AE signals of CFRP step lap joints featuring various pinning patterns were monitored and collected during tensile testing to identify the mechanisms of damage and assess the effectiveness of Z-pins and staple pins in particular in enhancing the structural performance of CFRP composites.

The novelty lies in the exploration of staples as a through thickness reinforcement method, particularly in comparison with traditional z-pinning method, by systematically evaluating the effectiveness and performance of staples in this particular situation. Staples are distinguished by their unusual, unique U-shaped geometry with dual through-thickness arms and a horizontal clamping mechanism, in contrast to z-pins, which may be limited by their single vertical line configurations. This work presents a new perspective on the strengthening of composite materials.

Fig. 2. Experimental test setup for the pinned composite tensile specimens.

2. Experimental procedures

2.1. Materials

The single step joints composite laminates were made of unidirectional carbon/epoxy prepreg (HS150/ER450; CIT, Legnano, Italy) tape prepared by the hand lay-up technique. The laminates stacking sequence was $[0°/90°/0°/90°/0°]_s$. Three groups of specimens were manufactured, namely: Z1 (unpinned), Z6 (z-pinned), and Z9 (staple-pinned) as shown in Fig. 1. Single stepped-lap joints were bonded together through a co-curing process, without the use of an additional adhesive layer, with an overlap length of 40 mm and overlap adherend thickness of 0.625 mm which is half the thickness of the sample. Preceding the curing phase, the integration of z-pins involved a manual insertion process into pre-punched holes, each crafted with a needle measuring 0.5 mm in diameter, ensuring alignment along the thickness direction. These pins were made of a continuous steel wire (0.5 mm diameter) known for its excellent corrosion resistance and heat resistance. Once inserted, the wires were cut to the laminate thickness just above the joint surfaces. Two distinct pinning configurations were selected to reinforce the overlap region of the joint panels. The first pinning configuration consisted of two rows of z-pinned at a distance of 5 mm from the edge of the overlap region (Fig. 1b). The second pinning configuration (Fig. 1c) consisted of two rows of staple pins with the same distance from the edge of the overlap's regions (taking into account that the two rows of staples were placed on opposite sides on the surface). A consistent 5 mm spacing between consecutive pins/staples along each row was upheld. As reference specimens, lap joints without staples or pins were created and cured in the same manner as the pinned samples. Following the reinforcing process, all joints underwent curing within an autoclave, subjected to a maximum temperature of 125 °C and a pressure of 3 bar. Upon completion of the curing process, the consolidated jointed panels were cut into samples 20 mm wide, 360 mm long, with an average thickness of 1.25 mm. The elastic properties of the carbon/epoxy were determined during tensile test and were as follows: $E_1 = 120$ GPa; $E_2 = 9.2$ GPa; $\nu_{12} = 0.26$; $G_{12} = 4$ GPa.

2.2. Experimental tensile test

Experimental tensile tests (Fig. 2) were carried out on Shimadzu ASG-X tensile testing machine equipped with 10 kN load cell. Prior to experiments, tabs were fastened on both sides to the composites at a length of 40 mm. To ensure quasi-static loading conditions, all tests were conducted with constant crosshead velocity equal to 1 mm/min. Prior to experiments, a millimeter paper was glued to samples in order to increase precise measurement of developing cracks that were recorded with a Nikon D500 4 K photo camera (Nikon, Tokyo, Japan).

Visual inspection technique was adopted to detect and measure the crack length growth. The camera was mounted at a fixed distance from the sample. An additional lamp was positioned around the sample to ensure optimal lighting conditions and minimize shadows. Images of the samples were taken at regular intervals during the recording of loading process. The crack length was measured by tracking the crack tip. The accuracy of the crack length measurements was determined to be ± 0.2 mm based on repeated measurements.

The acoustic emission signals generated by developing cracks were registered by using the Vallen AMSY-5 measurement system consisting of pre-amplifier (AEP-4, 34 dB of gain) and analog-to-digital (A/D) card (Vallen's ASIP-2, sampling frequency 40 MHz, resolution—18 bits, band width 1.6–2400 kHz). Piezoelectric sensors (Fujicera 1045S, max. freq. 1.3 MHz) were adhesively bonded to the top surface of the samples (Fig. 3) at the distance of 130 mm from specimen's end at 50 mm from the laminate center, where the lap-joint was located.

The load and AE responses were registered in real time at a 5 MHz sampling rate. Subsequently, the load–displacement vs cumulative energy and cumulative hits plots were created. In order to distinguish different damage failure mechanisms occurring during experimental tests, two different machine learning clustering techniques were utilized. After the experimental test, the failure surfaces were examined using the Keyence VHX-5000 microscope (Fig. 4).

2.3. Application of machine learning technique to identification of the acoustic signature of damage mechanisms

In composite structures different damage phenomena such as delamination, matrix cracking fiber debonding or fiber pull-out can occur during lifetime operation. The type of damage may depend on various factors such as resin and fiber materials, specific loading condition, loading rate or even humidity. The occurrence of different failures and their extent have influence on the structure integrity. Therefore, proper identification and recognition of damage types can

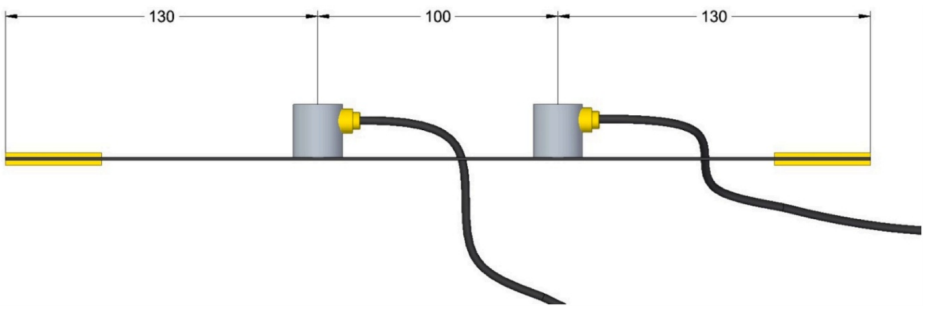

Fig. 3. Sensors positions on the test specimen.

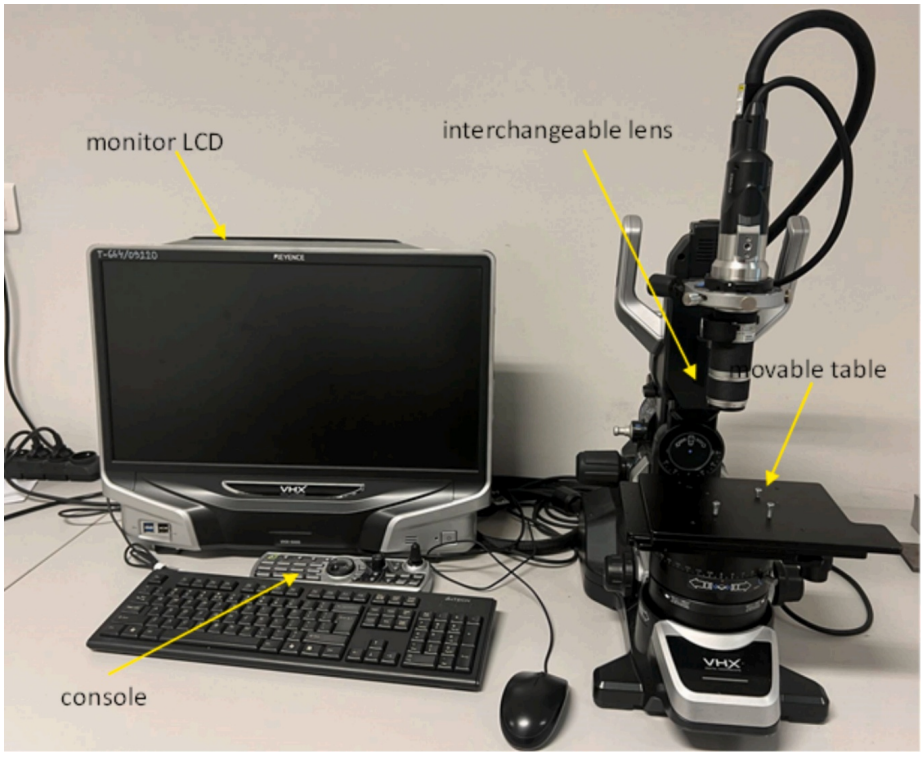

Fig. 4. The Keyence 5000 VHX microscope.

deliver important information about the state of the structure and can improve predictive prognosis models that aim to estimate the operating time of a system before failure. In this case, to realize this task, a synthesis of the acoustic emission technique and machine learning algorithms can have promising capability. In the current paper, identification and assignment of the acoustic emission signals signatures to different types of damages occurring during tensile tests of lap-joints laminates was done by using the unsupervised pattern recognition technique. Cluster analysis aimed to utilize machine learning algorithms for grouping acoustic emission patterns (extracted AE typical waveform features) into *N* classes corresponding to different failure mechanisms.

As indicated by the extensive literature review [57–64] each of the acoustic emission signals propagates inside a composite material with unique waveform features. For example, delamination is characterized by long duration time and low peak frequency, matrix cracking is determined by shorter rise time and duration, as well as lower peak frequency. On the other hand, fibers breaking is usually determined by high frequency and amplitude, as well as short rise time. The precise boundary values of aforementioned AE parameters are difficult to be generally specified due to discrepancies caused by such factors as: type of sensors used, applied loading conditions, sensor's positions or material attenuation. In current research, recorded AE signals were clustered

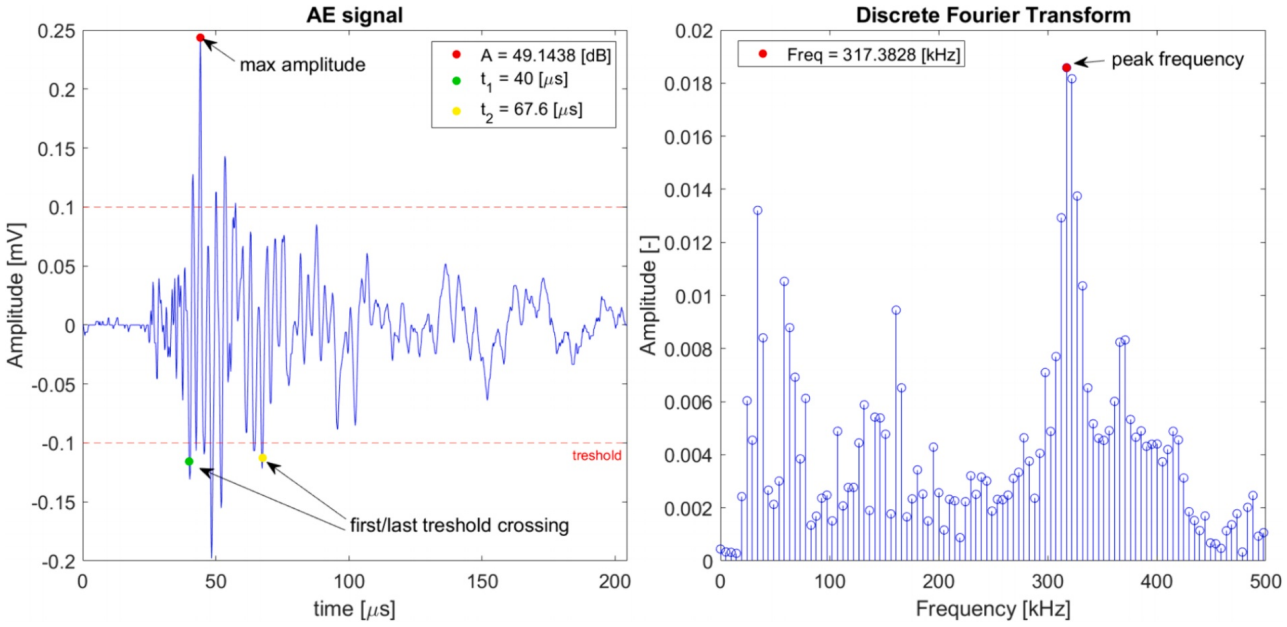

Fig. 5. Typical AE signal registered during tensile test and its spectral representation.

into three groups representing the most expected damage modes occurring during tensile tests of lap-joint laminates: delamination, matrix cracking and other failure mechanism related with deformation and damage of steel pins, as well as regions around it. For the last case, to better recognition of possible failure modes, a scanning electron microscopy observation should be performed, which is not the object of this paper. After clustering procedure, the partitioned acoustic emission signal features were referred to comparative values (resulted from literature review) obtained by other researchers. This allowed to predict and assign specific clusters to characteristic composite damage modes. The general procedure of signal registration and analysis was divided into three steps: collection of the AE data, preprocessing and converting the data into a usable form and sorting into groups called class. In the case of unsupervised pattern recognition, it is a process by which AE waveform features were classified in general group according to their similarity. With regard to the first step, the acoustic emission transient waves propagated into loaded lap-joint laminates were registered by using piezoelectric transducers attached to the specimen's top surface in the form of voltage versus time responses. All signals were registered by using the Vallen AMSY-5 acoustic emission system and were stored in two databases containing primary features and transient data. The registered signals were preliminary filtered to remove measurement noise. The weakest AE transient elastic waves for which the number of threshold crossing was less or equal to three were not taken into account for further considerations. Subsequently, six waveform features were extracted from each of the registered AE signals, namely: amplitude A [dB], rise time R [μs], energy E [aJ] (atto-Joule), duration D [μs], number of threshold crossing C (number of counts), and maximum frequency f [kHz] obtained by application of the FFT transform to raw signal. One of the acoustic emission signals registered during the experiment with typical waveform features is presented in Fig. 5.

Those six quantification AE features are often used in literature [54,65–67] to discriminate damage mechanisms in loaded composite materials. Therefore, it was decided to utilize them as an input data set collected in the form of pattern matrix. This matrix contains the whole input data set consisting of each acoustic emission hit and corresponding extracted waveform features. Subsequent steps in patter recognition process were feature normalization and eigenvector projection. For the first one, this procedure provides data normalization by scaling the AE features values by using the Equation (1):

$$AE_{norm} = \frac{AE - \min(AE)}{\max(AE) - \min(AE)} \tag{1}$$

The second mathematical procedure allows for decreasing the dimensionality of the feature space. In this case, the principal component analysis, that bases on reducing the input data vector to the most essential feature was used. In order to assign the AE waveform signal to a specific group representing a characteristic failure mechanism two unsupervised machine learning clustering techniques were utilized: the k-means and the Gaussian mixture model (GMM). Due to low computational cost those methods are the most commonly used clustering algorithms to partition data sets into groups. Two methods were chosen in order to compare cases. The machine learning algorithms were implemented in MatLab 2024 software where all data was processed. The first clustering method is an iterative procedure aiming to minimize the sum of squared error of the L_2 loss function:

$$L_2 = \sum_{j=1}^{k} \sum_{i} |u_j - x_i|^2 \tag{2}$$

Here the u_j is the center of cluster j {1, 2, k, ……} and x_i are the AE data points correlated with cluster j. The process star from initial cluster centers defined by random selection among the available data. Then the feature vectors are labeled in accordance with the closest calculated centroid and finally the labeled data center is calculated and the respective centroids are moved. The above procedures are repeated until the L_2 criterion is reached. The second GMM method is a multivariate Gaussian distribution that determine the probability that given AE data point belongs to a specific cluster by following equation:

$$p(x_j|\lambda) = \sum_{i=1}^{M} w_i g_i(x_j|u_i, \sum i) \tag{3}$$

Here M is a number of Gaussian components and w_i is the weight correlated with the multivariate Gaussian distribution g_i (Equation (4). Each component is defined by its mean and covariance values. The mixture is defined by a vector of mixing proportions that represents the fraction of the population described by a corresponding component.

$$g_i(x_i|u_i, \sum i) = \frac{1}{(2\pi^{d/2})|\sum i|^{1/2}} \exp\left(-\frac{1}{2}(x_j - u_i)^T \sum i^{-1}(x_j - u_i) \right) \tag{4}$$

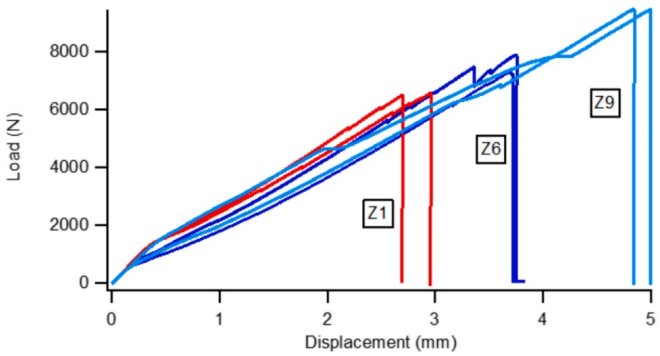

Fig. 6. Load vs displacement curves of unpinned, z-pinned and staple pinned joints under static tensile test.

3. Results and discussion

3.1. Tensile test

The load–displacement curves for the lap joints measured during static tensile loading for unpinned, z-pinned and stapled specimens are presented in Fig. 6. Most of the displacement spectrum showed primarily linear characteristics for the unpinned joint (Z1). The failure ultimately occurred at a load of 6.4 kN and manifested as essentially brittle fracture debonding cracks. Damage initiated by cracks at the end of the bonded region where the localized geometric stress concentration existed, that in turn excited the evolution of delamination. After reaching a critical value, the delamination propagated and resulted in a sudden complete separation of the two adherends. The failure of z-pinned joints (Z6) was governed by the same sequence of failure events observed in unpinned joints. However, the load–displacement curve revealed that the final separation of the z-pinned joints is preceded by a more progressive fracture process, during which the growth of the interfacial crack proceeded in steps. This advancement is attributed to the restraining effect of through-thickness z-pins, which reduce the energy available at the front of the crack and thus arrest or delay its propagation. Remarkably, the load and displacement range were the highest for the single lap joint with staples (Z9). It can be concluded that the introduction of staples within the structure did not entirely prevent delamination but significantly delayed its propagation. This delay is primarily attributed to the unique bridging mechanism of the staples, which effectively distribute stress across the overlapped layers of the material upon delamination initiation. By connecting the fractured zones and so reducing stress at the crack tips, staples reduced the driving force for propagation. Staples' clamping force fortified the bond between layers and increased resistance to layer separation. Even though delamination may still happen under stress, the stapled reinforcement of Z9 samples helped improve structural integrity and prolong its load-carrying capacity.

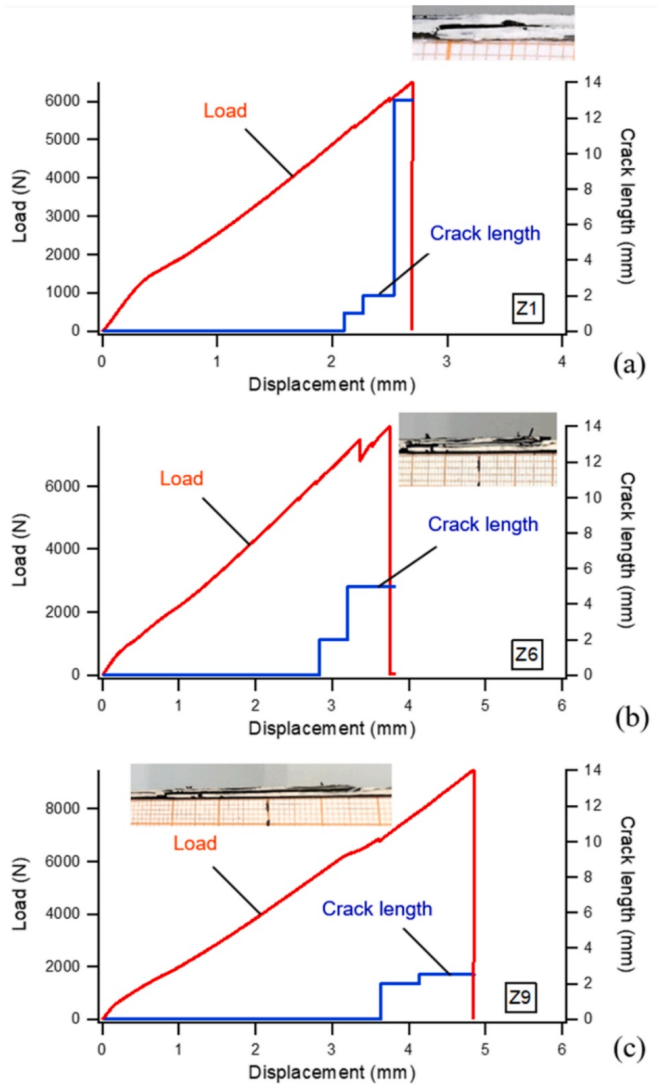

Fig. 7. Typical growth of total crack length: (a) Unpinned, (b) z-pinned, and (c) Staple pinned.

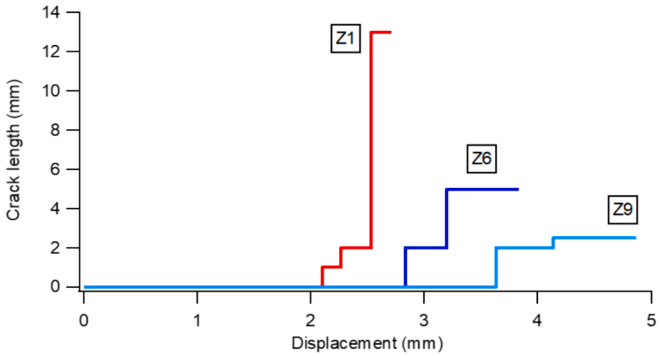

Fig. 8. Comparison of total crack length growth of the different configurations.

The typical growth of total crack which is the total length from the two edges of unpinned, z-pinned, and staple-pinned joints is illustrated in Fig. 7. The growth of crack length curve for unpinned joint in Fig. 7a was very fast and the crack length immediately before final failure is very large. The rapid rise indicated almost instantaneous crack propagation. While Fig. 7b depicting the z-pinned joint, showed a similar trend of increasing crack length, albeit at a somewhat slower rate compared to the unpinned specimens and with almost half the crack length at failure, which means that pins restrained the growth of cracks. However, despite the presence of z-pins, there were still instances of sudden jumps in crack length. In contrast, Fig. 7c for staple-pinned specimens demonstrated a distinct behavior. The crack length started to increase at a later stage compared to the other configurations and the rate of crack growth is significantly slower. The efficacy of staples in limiting crack length propagation has been shown by the delayed increase in crack length. The intimate contact promoted by the clamping action of staples leads to a reduction in overall crack length prior to failure, indicating superior crack restraint compared to both the unpinned and z-pinned configurations. The comparison is demonstrated in Fig. 8. For these three configurations, it appears that while both z-pins and staples contributed to restraining crack growth, staples emerged as the more effective solution. Their gripping action promoted intimate contact between layers, significantly minimized the rate of crack propagation and eventually led to an inferior crack length at failure compared to the other configurations.

3.2. Detection of damage onset by using acoustic emission technique

One of the goal of this paper was precise detection of damage initiation in lap-joint composite laminates by using the acoustic emission technique. The main advantage of this method is high sensitivity to detect material degradation at an early stage. It should be mentioned that this technique was previously successfully utilized by the authors of this article to detect initiation of delamination in elastically coupled DCB and ENF composite laminates [68–70]. In this case, the registered AE features were combined with load values registered during mechanical tests in real time. In order to detect damage onset, two different initiation criteria were used, namely: the cumulative energy and the cumulative hits. With regard to the above, the moment of damage initiation is considered when the first pronounced increase of those cumulative plots is observed. In Figs. 9-11 the load-time versus cumulative hits and cumulative energy curves obtained during tensile tests conducted on composite lap-joint laminates are presented. The AE points marked on the plots represent moments in which sudden increase in the gradients of cumulative values were observed. Hence, the aforementioned criteria were fulfilled. For those points, specific values of time and corresponding load were precisely determined. In the case of Z1 laminate significant increase for cumulated acoustic energy was observed at $t =$ 69 s of the test duration, corresponding to a load of 2516 N. In the case of laminate Z6 increase was observed at 124 s of the test, corresponding to a load of 4310 N. For the Z9 laminate respective values of time and load for significant increase were 81 s and 2348 N. These AE points represent moments in which crack propagation started. On the other hand, the increased rise in the cumulative number of hits indicates much faster propagation of delamination. The AE points for cumulated hits were as follows Z1: $t = 29$ s, F=1335 N, Z6: $t = 52$ s, F=1854 N, Z9: $t = 21$ s, F=697 N. It is also worth emphasizing that higher levels of cumulated acoustic energy activity were observed before the maximum load and before visually observed crack growth. In Fig. 10 at a load of 7461 N energy activity suddenly drops and no energy is released that can be correlated with visually noticed crack length increase (Fig. 7) and is it possible that pins stopped further crack growth. During loading Z9 sample it is also noticeable that a slight drop of load occurred with simultaneous high increase of energy release. Crack increased during that loading, but there was no further decrease in load value, which may be to the staples carrying staples carrying the load. For all samples, sudden increases in cumulative energy and cumulative hits occurred just before the final failure.

3.3. Recognition of damage mechanisms by using the machine learning techniques

Identification of acoustic emission signatures corresponding to

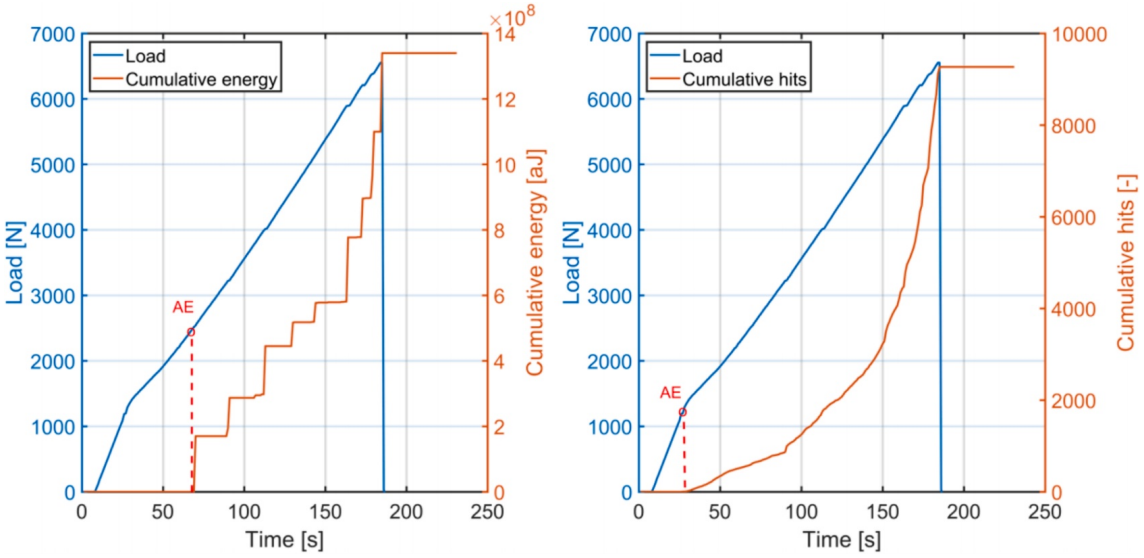

Fig. 9. Load-time plots versus: a) cumulative energy, b) cumulative hits, obtained for Z1 laminate subjected to tensile test.

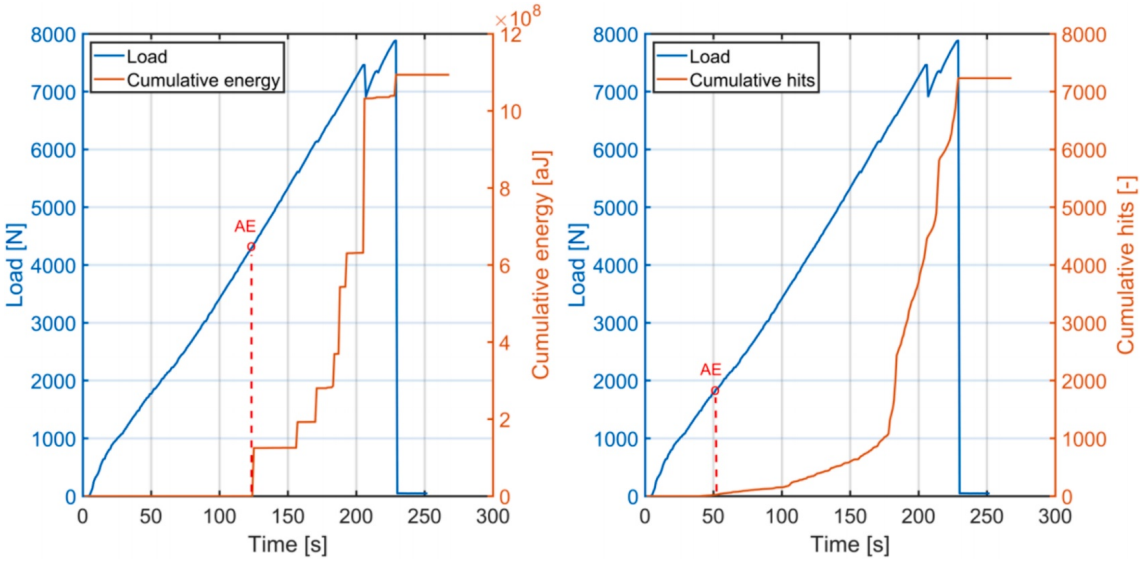

Fig. 10. Load-time plots versus: a) cumulative energy, b) cumulative hits, obtained for Z6 laminate subjected to tensile test.

characteristic damage modes were prepared based on the AE data collected during tensile tests conducted on the three types of the lap-joint laminates, namely: the Z1 unpinned, the Z6 pinned and the Z9 stapled specimens. All of the AE hits captured by piezoelectric sensors were transformed from analog to digital form and collected in the Vallen AE Software. The total numbers of the AE events registered by the two sensors were 9266, 7233 and 13,324 for unpinned, pinned and stapled laminates respectively. Subsequently, the characteristic signal features as: amplitude A [dB], rise time R [μs], energy E [aJ], duration D [μs], number of counts C and maximum frequency f [kHz] – (calculated by using the discrete Fourier transform) were extracted from each registered waveform and sent to Matlab Software. The first step covered preprocessing of extracted AE signatures including removing outliers and data normalization. Preliminary processed AE features in the form of plot matrix and its mutual correlation coefficients obtained for the Z1 laminate are presented in Fig. 12 and Table 1. The scatter plots provided insight into the quantitative data distribution and allowed for the assessment of possible linear correlations between multiple variables. Based on the histogram plots, it can be observed that most of the registered acoustic emission events were characterized by signal signatures exhibiting specific ranges, namely: amplitude (40 dB – 60 dB), rise time (0 – 20 μs), energy (0—200 aJ), duration (0—300 μs), number of counts (0–25) and peak frequency (0 – 300 kHz). In addition, mutual correlations can be observed between specific variables that indicate possible redundancy of data. The correlation coefficients reach values between −1 and 1 (0 – no correlation, −1/1 negative/positive correlation), which describes a linear relationship between measured variables. Based on values collected in Table 1 it can be noticed that energy values are strongly correlated with amplitude, duration and number of counts. Similarly, the number of threshold crossing C has a high correlation with A, E and D features. On the other hand, the frequency descriptors exhibit no correlation with other parameters. The presence of highly correlated variables increases the dimensionality of feature space and may decrease the classifier efficiency. This is the one of the greatest difficulties in multivariate statistical analysis that can be simplified by using additional mathematical processing that allows reducing redundant data and present it as a new set of uncorrelated variables. In this case, the principal component analysis was applied to all the AE feature data set. As a

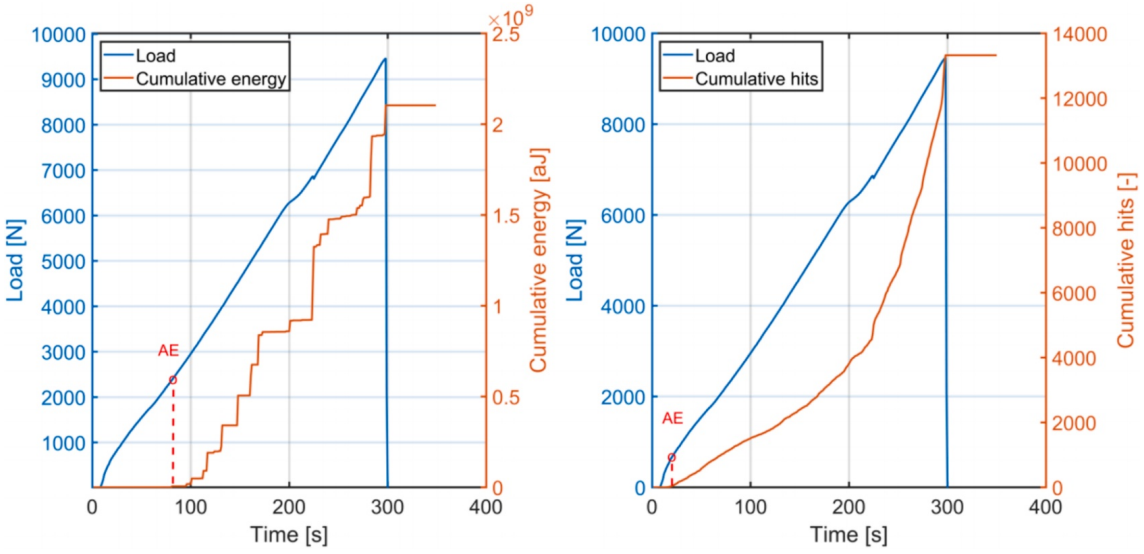

Fig. 11. Load-time plots versus: a) cumulative energy, b) cumulative hits, obtained for Z9 laminate subjected to tensile test.

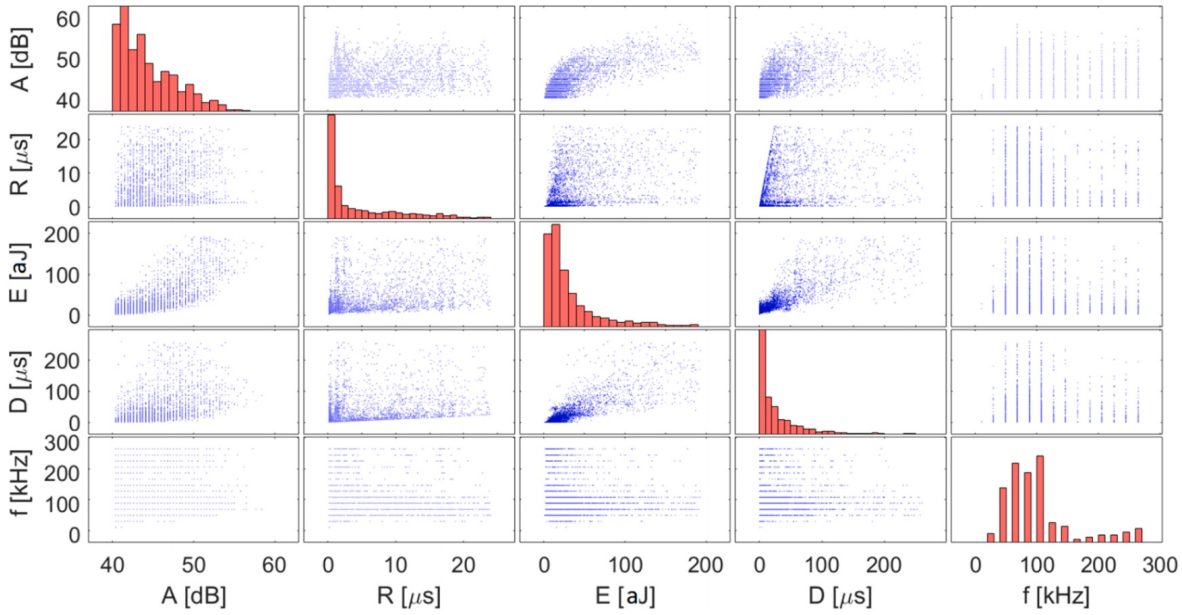

Fig.12. Typical scatter plots of AE waveform features data obtained for Z1 laminate subjected to tensile loading.

Table 1
Correlation coefficient values between different acoustic emission waveform features for Z1 laminate.

AE feature	*A* [dB]	*R* [μs]	*E* [aJ]	*D* [μs]	*C* [-]	*f* [kHz]
***A* [dB]**	1	0.3714	0.7620	0.5617	0.7891	0.0714
***R* [μs]**	0.3714	1	0.4333	0.3449	0.2920	−0.0960
***E* [aJ]**	0.7620	0.4333	1	0.8100	0.8237	−0.0916
***D* [μs]**	0.5617	0.3449	0.8100	1	0.7286	−0.0461
***C* [-]**	0.7891	0.2920	0.8237	0.7286	1	0.0411
***f* [kHz]**	0.0714	−0.0960	−0.0916	−0.0461	0.0411	1

result of this operation, the input feature vector was linearly transformed from a six dimensional to a four-dimensional space retaining maximum information about the input variables. The clustering procedure was prepared by using two different machine learning techniques, namely: the *k*-means and the Gaussian mixture model techniques. The clusters centroids were measured by using the squared euclidean distance metric technique. In addition, the number of iterations was set to 80. Moreover, a regularization parameter was established to 0.15. The clustering procedure was prepared on three AE datasets collected during tensile tests conducted on unpinned Z1, pinned Z6 and stapled Z9 laminates. The number of clusters *n* was chosen based on the tested composite type and the expected failure modes. They were as follows: for Z1 laminate *n* set to 2 (expected main damages: matrix cracking and delamination), for Z6 and Z9 *n* was equal to 3 (expected main damages: matrix cracking, delamination and other failure related with damage of steel pins and area around it).

The predictive labeling of clusters to a specific type of damage was done by relating the average values of the acoustic emission waveform features representing each group with typical ranges of those parameters that are characteristic for specific damage modes. The recommendations about distinctive AE signatures resulting from previous research conducted by the authors of current paper [56] and from extensive review of

Table 2
Mean values of the AE features obtained by using *k*-means technique for the Z1 laminate.

Cluster	*A* [dB]	*R* [μs]	*E* [aJ]	*D* [μs]	*C* [-]	*f* [kHz]	Percentage [%]	Predicted failure mode
1	54	19	376	259	16	369	28	delamination
2	48	13	69	75	6	331	72	matrix cracking

Table 3
Mean values of the AE features obtained by using GMM technique for the Z1 laminate.

Cluster	*A* [dB]	*R* [μs]	*E* [aJ]	*D* [μs]	*C* [-]	*f* [kHz]	Percentage [%]	Predicted failure mode
1	54	19	356	250	15	364	32	delamination
2	48	13	64	71	5	331	68	matrix cracking

Table 4
Mean values of the AE features obtained by using *k*-means technique for the Z6 laminate.

Cluster	*A* [dB]	*R* [μs]	*E* [aJ]	*D* [μs]	*C* [-]	*f* [kHz]	Percentage [%]	Predicted failure mode
1	58	23	879	339	19	338	18	other failure mechanisms
2	53	20	263	186	12	324	30	delamination
3	48	9	51	51	5	323	53	matrix cracking

Table 5
Mean values of the AE features obtained by using GMM technique for the Z6 laminate.

Cluster	*A* [dB]	*R* [μs]	*E* [aJ]	*D* [μs]	*C* [-]	*f* [kHz]	Percentage [%]	Predicted failure
1	58	23	864	335	19	337	18	other failure mechanisms
2	53	22	262	192	12	321	27	delamination
3	48	9	55	52	5	325	55	matrix cracking

Table 6
Mean values of the AE features obtained by using *k*-means technique for the Z9 laminate.

Cluster	*A* [dB]	*R* [μs]	*E* [aJ]	*D* [μs]	*C* [-]	*f* [kHz]	Percentage [%]	Predicted failure
1	55	31	392	206	13	306	17	other failure mechanisms
2	51	27	142	106	8	306	33	delamination
3	46	11	40	42	4	319	50	matrix cracking

Table 7
Mean values of the AE features obtained by using GMM technique For the Z9 laminate.

Cluster	***A*** **[dB]**	***R*** **[μs]**	***E*** **[aJ]**	***D*** **[μs]**	***C*** **[-]**	***f*** **[kHz]**	**Percentage [%]**	**Predicted failure**
1	55	30	414	205	13	307	15	other failure mechanisms
2	51	28	162	124	9	305	27	delamination
3	47	14	46	45	5	317	57	matrix cracking

state of the art where many researchers deeply investigated the issues of different damage phenomena identification by using the acoustic emission technique and the machine learning clustering algorithms. Considering the above, the shape of propagated elastic transient waveform generated by developing damage inside the material depends on the type of failure mechanism. Moreover, the signal primary features can also be correlated with characteristic damage type. Hence, for example, a matrix cracking phenomenon can be characterized by low energy and short duration. Similarly, delamination can be described by AE signals with longer rise time and with greater number of threshold crossing (counts). The more detailed discussion about general behavior of elastic waves induced by internal damage was described in the previous section. In the Tables (2 – 7) the results of clustering procedure prepared on the typical waveform features extracted from registered acoustic emission signals during the tensile tests conducted on the Z1, Z6 and Z9 laminates were presented. Those outcomes contain average values of the

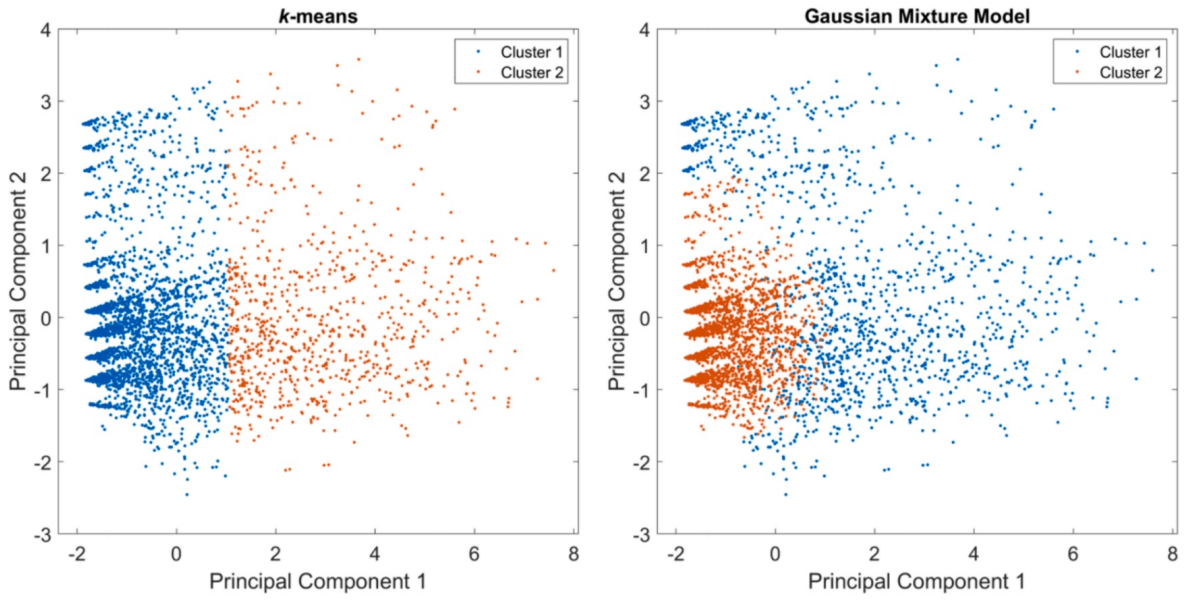

Fig. 13. Scatter plots of clustered waveform features extracted from the AE signals registered during tensile test of Z1 unpinned composite laminate.

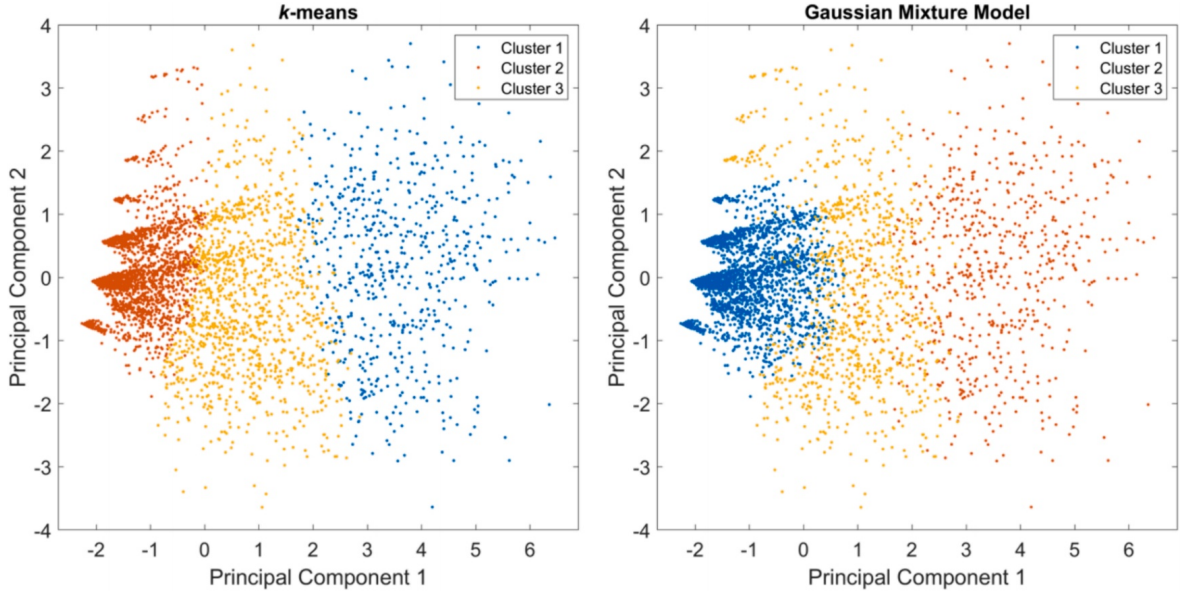

Fig. 14. Scatter plots of clustered waveform features extracted from the AE signals registered during tensile test of Z6 pinned composite laminate.

main AE features in each cluster, the predictive assignment of clustered data to failure mechanisms and its percentage contribution in AE data set obtained for specific test. The last parameter allows for quantitative estimation of damage presence in different types of lap-joint laminates under the static tensile test. To prepare comparative study the unsupervised machine learning grouping of the AE data was conducted by using two different clustering techniques: the *k*-means and the Gaussian mixture model. Those approaches gave similar average values of the AE features and its percentage contributions. Nevertheless, comparing the scatter plots (Figs. 13-15) obtained by using those techniques, the acoustic emission data were not grouped in the same manner. For the *k*-means algorithms the AE waveform features were partitioned in more pronounced clusters with less fuzziness at the boundaries than for the Gaussian mixture model. It should be noticed, that due to those approaches giving similar outcomes, the discussion about obtained results was conducted with respect to the values determined by using the *k*-means technique. In the case of the Z1 (unpinned) joints, two characteristic groups of signals that represent two failure mechanisms could be observed. They were as follows: cluster 1 corresponds to delamination (28 %) and cluster 2 corresponds to matrix cracking (72 %). For the Z6 (pinned) joint and Z9 (stapled) joint the collected AE data were divided into three characteristic clusters. For the Z6 laminate, damage phenomena caused by delamination (30 %), matrix cracking (53 %) and other failure mechanism (18 %) can be distinguished. The last failure group can be correlated with steel pins failure or laminate damage in the region around pin. Similar situation can be noticed for the Z9 stapled specimen. Here, the delamination group corresponded to 33 % of total AE signals, matrix cracking to 55 % and other failure mechanisms to 15 %. To sum up, the matrix cracking was found to be the most dominant mode of failure for all three groups of lap joint laminates (Z1, Z6, Z9) subjected to tensile loading. Delamination and other failure mechanisms were grouped in smaller clusters. Based on obtained outcomes, characteristic ranges of the AE waveform features with regard to predicted damage mechanisms can be established and they were as

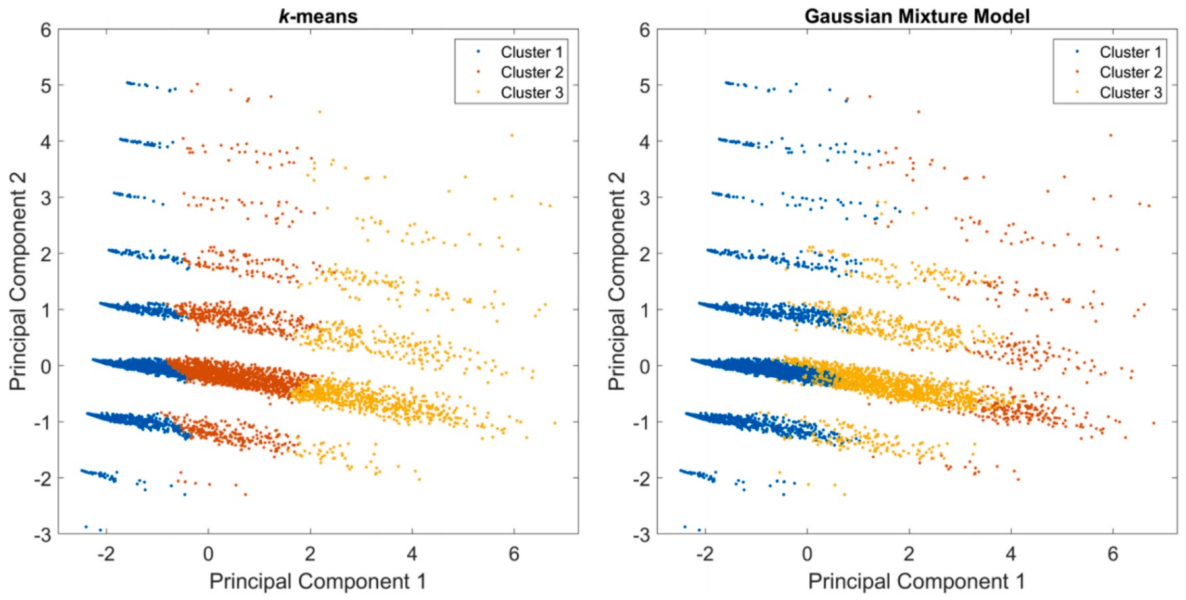

Fig. 15. Scatter plots of clustered waveform features extracted from the AE signals registered during tensile test of Z9 stapled composite laminate.

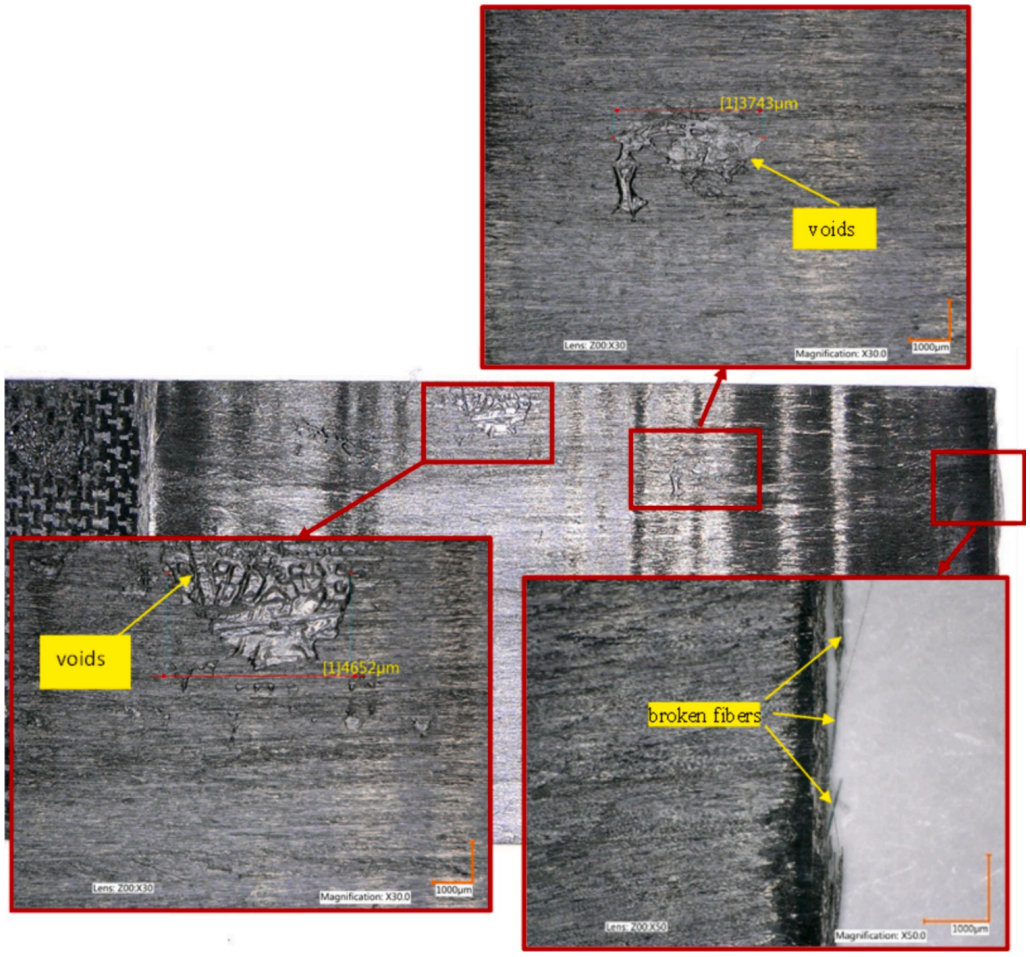

Fig. 16. Micrograph of Z1 unpinned specimen.

follows:

- for matrix cracking; *A* (46 – 48 dB), *R* (9 – 11 µs), *E* (40 – 69 aJ), *C* (4 – 6), D (42 – 75 µs) and *f* (319 – 331 kHz),
- for delamination: *A* (51 – 54 dB), *R* (19 – 27 µs), *E* (142 – 376 aJ), *C* (8 – 16), D (106 – 259 µs) and *f* (305 – 369 kHz)

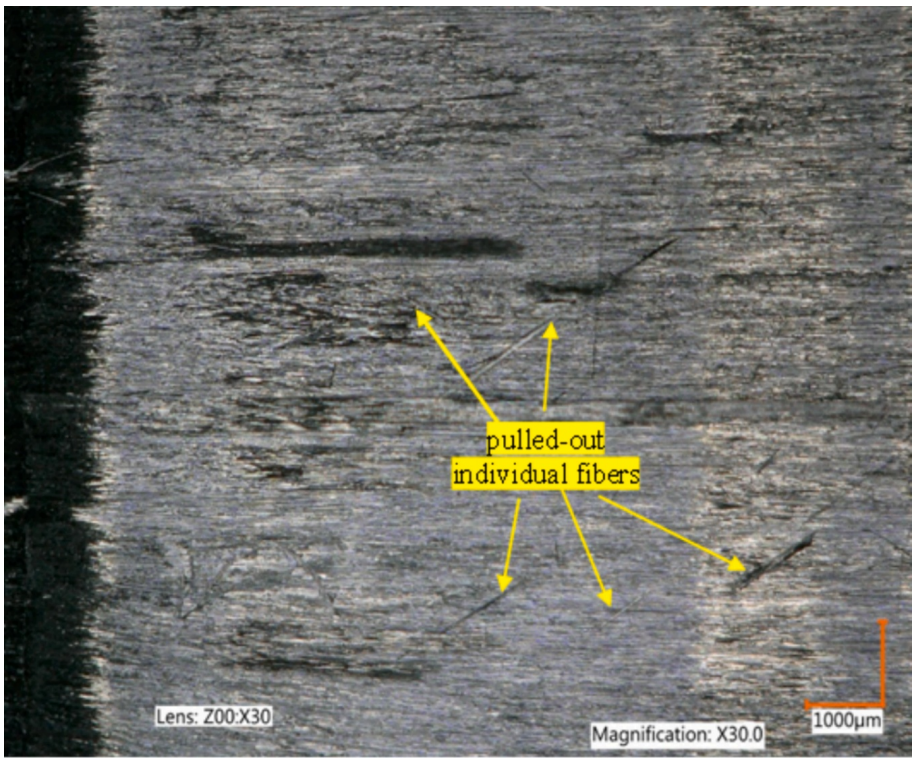

Fig. 17. Micrograph of the Z1 specimen fracture surface at 30x magnification.

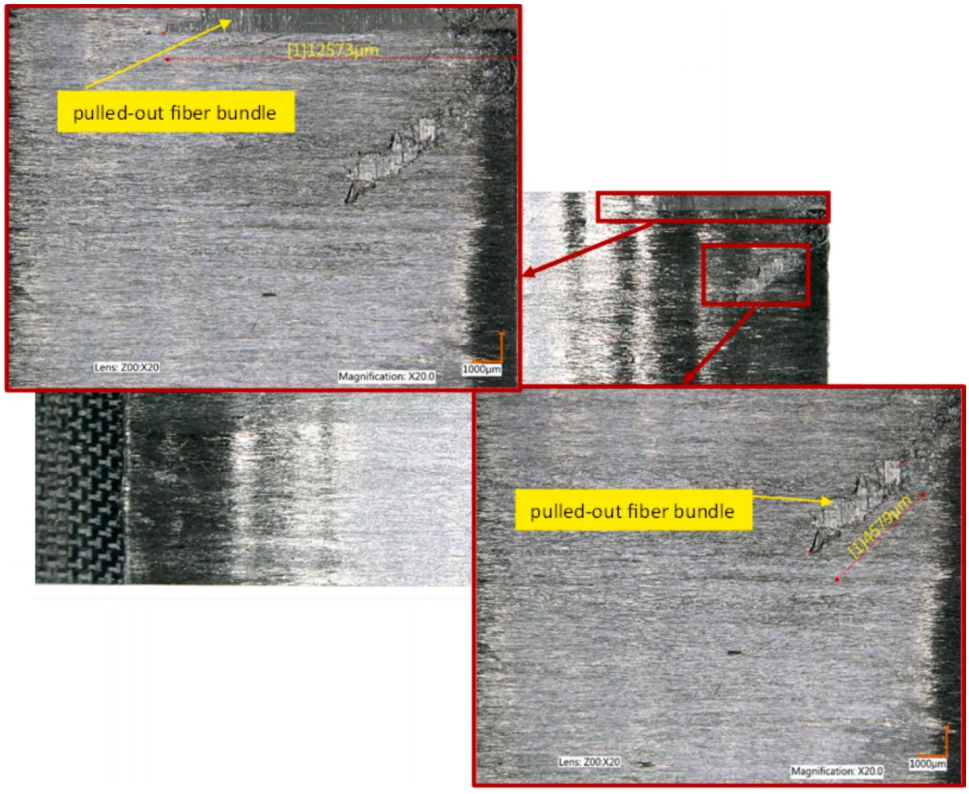

Fig. 18. Micrograph of Z-Pinned for Z6.

- for other failure mechanisms included pin damage: *A* (55 – 58 dB), *R* (23 – 31 µs), *E* (372 – 879 aJ), *C* (13 – 19), D (206 – 339 µs) and *f* (306 – 338 kHz)

For the last group, an additional future investigation is required for better recognition of the acoustic signatures mainly related with damage of steel pins.

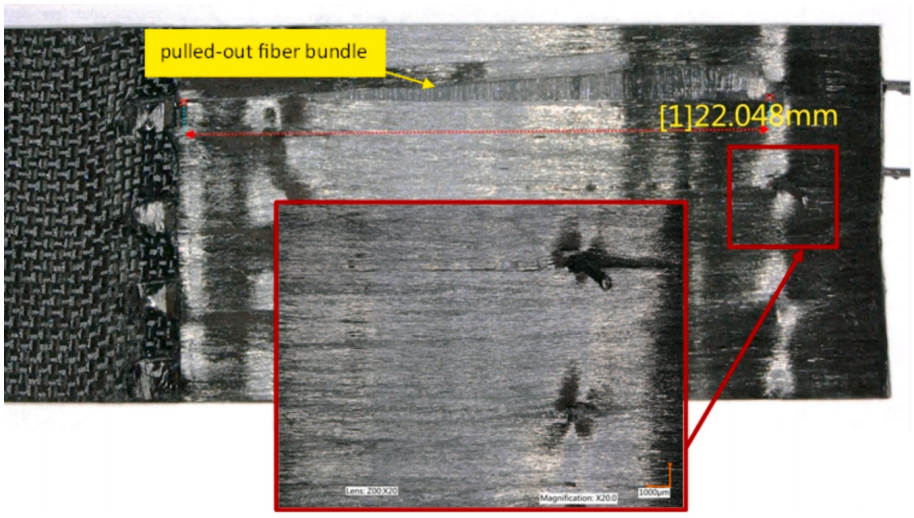

Fig. 19. Micrograph of Z9 staple pinned specimen.

3.4. Fractographic analysis

The appearance of fracture surfaces resulting from failure in longitudinal tension was primarily influenced by the bonding strength between fibers and matrix materials. To explain it simply, stronger bond between the fiber and matrix tends to produce a flatter fracture surface. Conversely, as the bond strength decreases the fracture surface becomes more irregular and fibrous. Understanding the quality of fiber matrix interface can provide valuable insights into the integrity of the structure. In Fig. 16 one can notice voids, which occur in the laminate due to the entrapment of volatile substances or air bubbles during the lay-up process. Additionally, they may arise from the entrapment of moisture during the crosslinking of the thermosetting matrix. When the laminate was subjected to tensile loading, these porosities and voids merge together forming cavities. Porosity can serve as a localized weakness and potentially leads to a decrease in delamination resistance. Moreover, by using magnification x30 it was possible to see several pulled-out individual fibers. Micrograph in Fig. 17 shows the broken end of the fiber appears frayed which suggests a tensile failure, where the fiber has been pulled apart.

In the Fig. 18 represents z-pinned joints, we may notice pulled-out fiber bundles where the fibers have been extracted from the resin matrix, which can be a result of mechanical stress. These disruptions are shown in two magnified insets providing a closer look at the damage. It was possible to measure real length 12573 μm and second 4579 μm of the dislodged fiber bundle. Such defects within the composite can compromise its structural integrity.

Fig. 19 represents the failure surface of a staple pinned joint, where broken pins are visible within the red square, together with pulled fiber bundles. spanning a total length of 22.048 mm, a cluster of carbon fibers detached from the matrix material upon rupture of the reinforcement. Such damages are significant and may indicate a weak point in the applied reinforcement staple pinned leading to the mass detachment of fibers from the material.

4. Conclusions

This study examined static tensile behavior of carbon/epoxy composite lap joints reinforced with steel z-pins and staples in the overlap region. Joints with 2 rows of pins and 2 rows of staples were manufactured to investigate the achievable performance improvements through different patterns of through thickness reinforcement. The main investigations provided can be summarized as follows:

- Z-pins and staples served in a strategic manner to slow down the growth of debonding cracks, enhanced the structural integrity and longevity. While staples appeared to be more efficace due to their special geometry, since they applied a clamping force across the overlapping layers, strengthened the bond between them by bridging delamination and reducing the driving force behind the growth of the cracks.
- Z-pins and staples have increased the load capacity and prolonged the displacement range for the composite materials until failure. The superior performance of staples over z-pins, however, indicates their potential as a cutting-edge strengthening method.
- During the analysis of the acoustic emission, a high level of cumulated acoustic energy was observed before the maximum point on the load–displacement plot and before visually observed crack movement. Using acoustic emission allows for earlier detection of degradation process. In further research more detailed analysis of acoustic emission and filtering signal will be conducted.
- Application of machine learning data clustering revealed that the fracture process was dominated by matrix cracking and delamination fracture mechanisms. The damage phenomena occurring around pin regions need to be more investigated in future tests.
- Through optical microscopy it was possible to observe the surface topography and morphology of the fracture after failure. The fractography illustrated how the staples and z-pins joint mitigate the propagation of debonding fractures at a microstructural level. Particularly, the fractography showed surfaces rich with voids, broken individual fibers. In the future deeper fractographic examination will be useful for scanning electron microscopy (SEM) to provide a more detailed understanding of the staple and pin interaction with the composite matrix and the resulting failure modes.

CRediT authorship contribution statement

Rayane El Mohtadi: Writing – original draft, Visualization, Resources, Methodology, Investigation, Data curation, Conceptualization. **Jakub Rzeczkowski:** Writing – review & editing, Writing – original draft, Validation, Software, Methodology, Investigation, Data curation, Conceptualization. **Izabela Korzec-Strzałka:** Writing – review & editing, Writing – original draft, Visualization, Validation, Software, Methodology, Investigation, Data curation. **Sylwester Samborski:** Writing – review & editing, Writing – original draft, Validation, Supervision, Methodology, Formal analysis, Conceptualization. **Francesco Aymerich:** Writing – review & editing, Writing – original draft, Validation, Supervision, Methodology, Formal analysis, Conceptualization.

Aleksander Czajka: Writing – original draft, Visualization, Methodology, Data curation.

Declaration of competing interest

The authors declare that they have no known competing financial interests or personal relationships that could have appeared to influence the work reported in this paper.

Data availability

Data will be made available on request.

Acknowledgement

The grant was financed in the framework of the pro-quality program of Lublin University of Technology „Grants for grants" 2/GnG/2023

References

[1] Da Silva LFM, Marques EAS, Campilho RDSG. Design Rules and Methods to Improve Joint Strength. In: Da Silva LFM, Öchsner A, Adams RD, editors. Handbook of Adhesion Technology. Cham: Springer International Publishing; 2018. p. 773–810.
[2] Banea MD, Da Silva LFM. Adhesively Bonded Joints in Composite Materials: An Overview. Proceedings of the Institution of Mechanical Engineers, Part L: Journal of Materials: Design and Applications 2009;223:1–18.
[3] Wisnom MR. The Role of Delamination in Failure of Fibre-Reinforced Composites. Phil Trans R Soc A 2012;370:1850–70.
[4] Huang T, Bobyr M. A Review of Delamination Damage of Composite Materials. J Compos Sci 2023;7:468.
[5] Blackman BRK. Delamination in Adhesively Bonded Joints. In Delamination Behaviour of Composites: Elsevier; 2008. p. 458–84.
[6] Potluri P, Hogg P, Arshad M, Jetavat D, Jamshidi P. Influence of Fibre Architecture on Impact Damage Tolerance in 3D Woven Composites. Appl Compos Mater 2012; 19:799–812.
[7] Warren KC, Lopez-Anido RA, Goering J. Experimental Investigation of Three-Dimensional Woven Composites. Compos A Appl Sci Manuf 2015;73:242–59.
[8] Mouritz AP, Bannister MK, Falzon PJ, Leong KH. Review of Applications for Advanced Three-Dimensional Fibre Textile Composites. Compos A Appl Sci Manuf 1999;30:1445–61.
[9] Kamiya R, Cheeseman BA, Popper P, Chou T-W. Some Recent Advances in the Fabrication and Design of Three-Dimensional Textile Preforms: A Review. Compos Sci Technol 2000;60:33–47.
[10] Mouritz AP. Review of Z-Pinned Composite Laminates. Compos A Appl Sci Manuf 2007;38:2383–97.
[11] Loi G, Buonadonna P, El Mohtadi R, Carta M, Lai D, El Mehtedi M, et al. Effect of Selective Z-Pinning on the Static and Fatigue Strength of Step Joints between Composite Adherends. J Compos Sci 2024;8:84.
[12] Pegorin F, Pingkarawat K, Daynes S, Mouritz AP. Influence of Z-Pin Length on the Delamination Fracture Toughness and Fatigue Resistance of Pinned Composites. Compos B Eng 2015;78:298–307.
[13] Partridge IK, Bonnington T, Cartié DDR. Manufacture and Performance of Z-Pinned. Composites 2003.
[14] Pingkarawat K, Mouritz AP. Improving the Mode I Delamination Fatigue Resistance of Composites Using Z-Pins. Compos Sci Technol 2014;92:70–6.
[15] Pegorin F, Pingkarawat K, Mouritz AP. Mixed-Mode I/II Delamination Fatigue Strengthening of Polymer Composites Using z-Pins. Compos B Eng 2017;123: 219–26.
[16] Partridge I, Cartie D. Delamination Resistant Laminates by Z-Fiber® Pinning: Part I Manufacture and Fracture Performance. Compos A Appl Sci Manuf 2005;36:55–64.
[17] Nogueira, A.C.; Drechsler, K.; Hombergsmeier, E. Analysis of the Static and Fatigue Strength of a Damage Tolerant 3D-Reinforced Joining Technology on Composite Single Lap Joints. In Proceedings of the 53rd AIAA/ASME/ASCE/AHS/ASC Structures, Structural Dynamics and Materials Conference
20th AIAA/ASME/AHS Adaptive Structures Conference
14th AIAA; American Institute of Aeronautics and Astronautics: Honolulu, Hawaii, April 23 2012.
[18] Bisagni C, Furfari D, Pacchione M. Experimental Investigation of Reinforced Bonded Joints for Composite Laminates. J Compos Mater 2018;52:431–47.
[19] Jürgens, M.; Nogueira, A.C.; Lang, H.; Hombergsmeier, E.; Drechsler, K. INFLUENCE OF AN OPTIMIZED 3D-REINFORCEMENT LAYOUT ON THE STRUCTURAL MECHANICS OF CO-BONDED CFRP JOINTS. **2014**.
[20] Juergens, M.; Kurtovic, A.; Mertens, T.; Kolb, M.; Greitemeier, D.; Lang, H.; Hombergsmeier, E.; Drechsler, K. Influence of surface treatment and design of 3d-reinforcements on delamination resistance & mechanical properties of CFRP/CFRP joints under static & fatigue loading. **2015**.
[21] Stelzer S, Ucsnik S, Pinter G. Fatigue Behaviour of Composite-Composite Joints Reinforced with Cold Metal Transfer Welded Pins. Int J Fatigue 2015;81:37–47.
[22] Stelzer S, Ucsnik S, Pinter G. Strength and Damage Tolerance of Composite-Composite Joints with Steel and Titanium through the Thickness Reinforcements. Compos A Appl Sci Manuf 2016;88:39–47.
[23] Mouritz AP, Cox BN. A Mechanistic Interpretation of the Comparative In-Plane Mechanical Properties of 3D Woven, Stitched and Pinned Composites. Compos A Appl Sci Manuf 2010;41:709–28.
[24] Cartié DDR, Troulis M, Partridge IK. Delamination of Z-Pinned Carbon Fibre Reinforced Laminates. Compos Sci Technol 2006;66:855–61.
[25] Zhang X, Hounslow L, Grassi M. Improvement of Low-Velocity Impact and Compression-after-Impact Performance by z-Fibre Pinning. Compos Sci Technol 2006;66:2785–94.
[26] Chang P, Mouritz AP, Cox BN. Properties and Failure Mechanisms of Pinned Composite Lap Joints in Monotonic and Cyclic Tension. Compos Sci Technol 2006; 66:2163–76.
[27] Chang P, Mouritz AP, Cox BN. Properties and Failure Mechanisms of Z-Pinned Laminates in Monotonic and Cyclic Tension. Compos A Appl Sci Manuf 2006;37: 1501–13.
[28] Sarantinos N, Tsantzalis S, Ucsnik S, Kostopoulos V. Review of Through-the-Thickness Reinforced Composites in Joints. Compos Struct 2019;229:111404.
[29] Mouritz AP. Review of Z-Pinned Laminates and Sandwich Composites. Compos A Appl Sci Manuf 2020;139:106128.
[30] Sachse, R.; Pickett, A.K.; Käß, M.; Middendorf, P. Numerical simulation of fatigue crack growth in the adhesive bondline of hybrid CFRP joints.
[31] Löbel T, Kolesnikov B, Scheffler S, Stahl A, Hühne C. Enhanced Tensile Strength of Composite Joints by Using Staple-like Pins: Working Principles and Experimental Validation. Compos Struct 2013;106:453–60.
[32] M'membe B, Yasaee M, Hallett SR, Partridge IK. Effective Use of Metallic Z-Pins for Composites' through-Thickness Reinforcement. Compos Sci Technol 2019;175: 77–84.
[33] Xu J, Wang W, Han Q, Liu X. Damage Pattern Recognition and Damage Evolution Analysis of Unidirectional CFRP Tendons under Tensile Loading Using Acoustic Emission Technology. Compos Struct 2020;238:111948.
[34] Garcea SC, Wang Y, Withers PJ. X-Ray Computed Tomography of Polymer Composites. Compos Sci Technol 2018;156:305–19.
[35] Dong J, Kim B, Locquet A, McKeon P, Declercq N, Citrin DS. Nondestructive Evaluation of Forced Delamination in Glass Fiber-Reinforced Composites by Terahertz and Ultrasonic Waves. Compos B Eng 2015;79:667–75.
[36] Heuer H, Schulze M, Pooch M, Gäbler S, Nocke A, Bardl G, et al. Review on Quality Assurance along the CFRP Value Chain – Non-Destructive Testing of Fabrics, Preforms and CFRP by HF Radio Wave Techniques. Compos B Eng 2015;77: 494–501.
[37] Libonati F, Vergani L. Damage Assessment of Composite Materials by Means of Thermographic Analyses. Compos B Eng 2013;50:82–90.
[38] Liang Q, Liu J, Wang X, Liu X, Zhang D, Qian K. Flexural Progressive Failure Mechanism of Hybrid 3D Woven Composites: Combination of X-Ray Tomography, Acoustic Emission and Digital Image Correlation. Compos Struct 2022;280: 114894.
[39] Djabali, A.; Toubal, L.; Zitoune, R.; Rechak, S. Fatigue Damage Evolution in Thick Composite Laminates: Combination of X-Ray Tomography, Acoustic Emission and Digital Image Correlation. Composites Science and Technology **2019**, 183, 107815Garcea, S.C.; Wang, Y.; Withers, P.J. X-Ray Computed Tomography of Polymer Composites. Composites Science and Technology **2018**, 156, 305–319.
[40] Silomon J, Gluch J, Clausner A, Paul J, Zschech E. Crack Identification and Evaluation in BEoL Stacks of Two Different Samples Utilizing Acoustic Emission Testing and Nano X-Ray Computed Tomography. Microelectron Reliab 2021;121: 114137.
[41] Pernigoni L, Lafont U, Grande AM. Self-Healing Materials for Space Applications: Overview of Present Development and Major Limitations. CEAS Space J 2021;13: 341–52.
[42] Brunner AJ, Blackman BRK, Davies P. A Status Report on Delamination Resistance Testing of Polymer-Matrix Composites. Eng Fract Mech 2008;75:2779–94.
[43] Saeedifar M, Fotouhi M, Ahmadi Najafabadi M, Hosseini Toudeshky H, Minak G. Prediction of Quasi-Static Delamination Onset and Growth in Laminated Composites by Acoustic Emission. Compos B Eng 2016;85:113–22.
[44] Crivelli D, Guagliano M, Eaton M, Pearson M, Al-Jumaili S, Holford K, et al. Localisation and Identification of Fatigue Matrix Cracking and Delamination in a Carbon Fibre Panel by Acoustic Emission. Compos B Eng 2015;74:1–12.
[45] Bohse J. Acoustic Emission Characteristics of Micro-Failure Processes in Polymer Blends and Composites. Compos Sci Technol 2000;60:1213–26.
[46] Komai, K., Minoshima, K., & Shibutani Investigations of the Fracture Mechanism of Carbon/Epoxy Composites by AE Signal Analyses.
[47] Godin N, Huguet S, Gaertner R, Salmon L. Clustering of Acoustic Emission Signals Collected during Tensile Tests on Unidirectional Glass/Polyester Composite Using Supervised and Unsupervised Classifiers. NDT and E Int 2004;37:253–64.
[48] Dos Santos Rolo T, Reich S, Karpov D, Gasilov S, Kunka D, Fohtung E, et al. A Shack-Hartmann Sensor for Single-Shot Multi-Contrast Imaging with Hard X-Rays. Appl Sci 2018;8:737.
[49] Ruiz J, Navarro P, Hernández M, Lucas M, Kaiser AS. Thermal Performance and Emissions Analysis of a New Cooling Tower Prototype. Appl Therm Eng 2022;206: 118065.
[50] Özaslan E, Yetgin A, Acar B, Güler MA. Damage Mode Identification of Open Hole Composite Laminates Based on Acoustic Emission and Digital Image Correlation Methods. Compos Struct 2021;274:114299.
[51] Xu D, Liu PF, Li JG, Chen ZP. Damage Mode Identification of Adhesive Composite Joints under Hygrothermal Environment Using Acoustic Emission and Machine Learning. Compos Struct 2019;211:351–63.

[52] Sause MGR, Schmitt S, Kalafat S. Failure Load Prediction for Fiber-Reinforced Composites Based on Acoustic Emission. Compos Sci Technol 2018;164:24–33.
[53] McCrory JP, Al-Jumaili SK, Crivelli D, Pearson MR, Eaton MJ, Featherston CA, et al. Damage Classification in Carbon Fibre Composites Using Acoustic Emission: A Comparison of Three Techniques. Compos B Eng 2015;68:424–30.
[54] Saeedifar M, Najafabadi MA, Zarouchas D, Toudeshky HH, Jalalvand M. Clustering of Interlaminar and Intralaminar Damages in Laminated Composites under Indentation Loading Using Acoustic Emission. Compos B Eng 2018;144:206–19.
[55] Bhat C, Bhat MR, Murthy CRL. Acoustic Emission Characterization of Failure Modes in Composites with ANN. Compos Struct 2003;61:213–20.
[56] Samborski S, Rzeczkowski J, Korzec-Strzałka I. Experimental Study of Delamination Process in Elastically Coupled Laminates with the Acoustic Emission Technique. Eng Struct 2024;300:117196.
[57] Fotouhi M, Suwarta P, Jalalvand M, Czel G, Wisnom MR. Detection of fibre fracture and ply fragmentation in thin-ply UD carbon/glass hybrid laminates using acoustic emission. Compos A Appl Sci Manuf 2016;86:66–76.
[58] Woo SC, Kim TW. High-strain-rate impact in Kevlar-woven composites and fracture analysis using acoustic emission. Compos B Eng 2014;60:125–36.
[59] Bourchak M, Farrow IR, Bond IP, Rowland CW, Menan F. Acoustic emission energy as a fatigue damage parameter for CFRP composites. Int J Fatigue 2007;29(3):457–70.
[60] Liu PF, Chu JK, Liu YL, Zheng JY. A study on the failure mechanisms of carbon fiber/epoxy composite laminates using acoustic emission. Mater Des 2012;37:228–35.
[61] Gong XL, Gong XJ, Laksimi A, Benzeggagh ML. Application of Tsai-Wu criterion to notched and Unnotched composite laminates under torque loading. J Compos Mater 2000;34(6):460–78.
[62] Barré S, Benzeggagh ML. On the use of acoustic emission to investigate damage mechanisms in glass-fibre-reinforced polypropylene. Compos Sci Technol 1994;52(3):369–76.
[63] Huang X, Yan X. Investigation of damage mechanisms in self-reinforced polyethylene composites by acoustic emission. Compos Sci Technol 2006;66(3-4):444–9.
[64] Ding P, Li Q, Huang X. Classification of acoustic emission sources produced by carbon/epoxy composite based on support vector machine. IOP Conference Series: Materials Science and Engineering 2015;Vol. 87. No. 1.
[65] Roundi W, El Mahi A, El Gharad A, Rebiere JL. Acoustic emission monitoring of damage progression in glass/epoxy composites during static and fatigue tensile tests. Appl Acoust 2018;132:124–34.
[66] Malpot A, Touchard F, Bergamo S. An investigation of the influence of moisture on fatigue damage mechanisms in a woven glass-fibre-reinforced PA66 composite using acoustic emission and infrared thermography. Compos B Eng 2017;130:11–20.
[67] Yousefi J, Najfabadi MA, Toudeshky HH, Akhlaghi M. Damage evaluation of laminated composite material using a new acoustic emission Lamb-based and finite element techniques. Appl Compos Mater 2018;25:1021–40.
[68] Rzeczkowski J, Samborski S. Experimental and numerical research of delamination process in CFRP laminates with bending-twisting elastic couplings. Materials 2022;15(21):7745.
[69] Rzeczkowski J, Samborski S, Prokopek K. Experimental determination of the mode I fracture toughness in FRP laminates with hybrid delamination interfaces. Advances in Science and Technology Research Journal 2022;16:5.
[70] Rzeczkowski J, Samborski S, de Moura M. Experimental investigation of delamination in composite continuous fiber-reinforced plastic laminates with elastic couplings. Materials 2020;13(22):5146.